Consistent and Elastic Registration of Histological Sections using Vector-Spline Regularization

Ignacio Arganda-Carreras[1,3] , Carlos O. S. Sorzano[1,5], Roberto Marabini[1,3], José María Carazo[1] , Carlos Ortiz-de-Solórzano[2], Jan Kybic[4]

[1] Biocomputing Unit, Nacional Centre of Biotechnology, Universidad Autónoma de Madrid, 28049 Cantoblanco, Madrid, Spain
{iarganda, coss, roberto, carazo}@cnb.uam.es
http://biocomp.cnb.uam.es/
[2] Cancer Imaging Laboratory, Centre for Applied Medical Research (CIMA), 31008 Pamplona, Spain
codesolorzano@unav.es
http://www.cima.es/index_english.html
[3] Escuela Politécnica Superior, Universidad Autónoma de Madrid, 28049 Madrid, Spain
{Ignacio.Arganda, Roberto.Marabini}@uam.es
http://www.ii.uam.es/esp/welcomii.php?idioma=eng
[4] Center for Machine Perception, Czech Technical University, 121 35 Prague 2, Czech Republic
kybic@fel.cvut.cz
http://cmp.felk.cvut.cz/
[5] Escuela Politécnica Superior, Univ. San Pablo CEU, 28003 Madrid, Spain
coss.eps@ceu.es
http://www.uspceu.com/

Abstract. Here we present a new image registration algorithm for the alignment of histological sections that combines the ideas of B-spline based elastic registration and consistent image registration, to allow simultaneous registration of images in two directions (direct and inverse). In principle, deformations based on B-splines are not invertible. The consistency term overcomes this limitation and allows registration of two images in a completely symmetric way. This extension of the elastic registration method simplifies the search for the optimum deformation and allows registering with no information about landmarks or deformation regularization. This approach can also be used as the first step to solve the problem of group-wise registration.

1 Introduction

Studying the three-dimensional organization of complex histological structures requires imaging, analyzing and registering large sets of images taken from serially sectioned tissue blocks. We have developed an integrated microscopy system that automates or greatly reduces the amount of interaction required for these tasks [1, 2] and provides volumetric renderings of the structures in the tissue.

Proper section alignment is the first step towards an accurate 3D tissue reconstruction, as it is in other imaging modalities [3, 4]. In our case we perform a coarse align-

ment of the sections using an automatic rigid-body registration method [5]. This method can not correct some non-linear distorting effects (e.g. tissue folding, stretching, tearing, etc.) caused by the manual sectioning process. Moreover, the distance between sections causes significant differences between the same structures of interest in consecutive sections, which could be misinterpreted by a complete linear registration process. Therefore, a non-linear or local method is strongly needed in order to refine the first registration step.

In this paper we present a new method for elastic and consistent registration of histological sections. All the examples described in the paper used mammary gland tissue samples; however, the same algorithm could be equally applied to other tissue sources and image modalities.

2 Methodology

In this work we combine the idea of elastic registration using vector-spline regularization [6] with that of a consistent registration [7]. We combine both ideas and extend them in order to overcome their limitations. The standard registration method presented in [6] propose the calculation of the elastic deformation field trough the minimization of an energy functional composed by three terms: the energy of the similarity error between both images (represented by the pixelwise mean-square distance), the error of the mapping of soft landmarks, and a regularization term based on the divergence and the curl of the deformation to ensure its smoothness. This minimization is optimized by a variant of the robust Levenberg-Marquardt method.

We transform the energy functional presented in [6] into a new functional that incorporates a factor of the deformation field consistency. Unlike in [6], we are now looking for two transformations at the same time (direct and inverse). Therefore, the vectors passed to the Levenberg-Marquardt optimizer are now twice as long. Besides the measurement of dissimilarity between the source and target images (now in both directions) E_{img}, the optional landmark constraint E_{μ} and the regularization term (E_{div} + E_{rot}), we add a new energy term E_{cons} that expresses the geometrical consistency between the elastic deformation in one direction (from source to target) and the other direction (from target to source). Therefore, the energy function present now four terms and is given by

$$E = w_i E_{img} + w_{\mu} E_{\mu} + \left(w_d E_{div} + w_r E_{rot} \right) + w_c E_{cons} \ . \qquad \textbf{(1)}$$

Where w_c is the specific weight given to the new consistency term.

2.1 Consistency Term

The consistency energy represents the geometrical distances between the pixel coordinates after applying both transformations (direct-inverse or inverse-direct), i.e. the amount by which the composed transformation differs from identity. The standard approach [6] for this type of registration is to find a deformation function

$$g^+(x):\mathbb{R}^2 \to \mathbb{R}^2 \ . \tag{2}$$

This function transforms the source image I_s into an image as similar as possible to the target image I_t. This transformation g^+ maps coordinates in I_s into coordinates in I_t. Here, following [7], we will also simultaneously look for its corresponding inverse function

$$g^-(x):\mathbb{R}^2 \to \mathbb{R}^2 \ . \tag{3}$$

This function maps the coordinates in I_t into coordinates in I_s.
Following this notation, our consistency energy term is given by

$$E_{cons} = E^+_{cons} + E^-_{cons} = \int_{\vec{x}\in\mathbb{R}^2} \left\| \vec{x} - g^-(g^+(\vec{x})) \right\|^2 d\vec{x} + \int_{\vec{x}\in\mathbb{R}^2} \left\| \vec{x} - g^+(g^-(\vec{x})) \right\|^2 d\vec{x} \ . \tag{4}$$

If we approximate the integrals by discrete sums and restrict the integration domain, we obtain

$$E^+_{cons} = \frac{1}{\#\Omega^+} \sum_{\vec{x}\in\Omega^+} \left\| \vec{x} - g^-(g^+(\vec{x})) \right\|^2 \ . \tag{5}$$

$$E^-_{cons} = \frac{1}{\#\Omega^-} \sum_{\vec{x}\in\Omega^-} \left\| \vec{x} - g^+(g^-(\vec{x})) \right\|^2 \ . \tag{6}$$

Where Ω^+, Ω^- define sets of relevant pixels common to the target and source images:

$$\Omega^+ = \left\{ \vec{x} \in \Omega_s \cap \mathbb{Z}^2 : g^+(\vec{x}) \in \Omega_t \cap \mathbb{Z}^2 \right\} \ . \tag{7}$$

$$\Omega^- = \left\{ \vec{x} \in \Omega_t \cap \mathbb{Z}^2 : g^-(\vec{x}) \in \Omega_s \cap \mathbb{Z}^2 \right\} \ . \tag{8}$$

And where $\#\Omega^+$ and $\#\Omega^-$ are the number of pixels in the masks.

2.2 Deformation Representation

Following [6] we represent the deformation fields as a linear combination of B-splines. For instance, g^+:

$$\begin{aligned} g^+(\vec{x}) &= g^+(x,y) \\ &= \left(g_1^+(x,y), g_2^+(x,y) \right) \\ &= \sum_{k,l\in\mathbb{Z}^2} \begin{pmatrix} c^+_{1,k,l} \\ c^+_{2,k,l} \end{pmatrix} \beta^3\left(\frac{x}{s_x} - k \right) \beta^3\left(\frac{y}{s_y} - l \right) \end{aligned} \tag{9}$$

Where s_x and s_y are scalars (sampling steps) controlling the degree of detail of the representation of the deformation field.

2.3 Explicit Derivatives

The chosen optimizer uses gradient information. We will now calculate the derivatives of the energy function with respect to all the parameters, starting with E_{cons}. It can be easily shown that the derivative of E^{+}_{cons} with respect to any of the deformation coefficients defining the first component (x in our case) of the direct deformation field g^{+}, is given by

$$\frac{\partial E^{+}_{cons}}{\partial c^{+}_{1,k,l}} = -2 \sum_{\vec{x} \in \Omega^{+}} \left(\vec{x} - g^{-}(g^{+}(\vec{x})) \right) \cdot \left(\frac{\partial}{\partial c^{+}_{1,k,l}} \left(g^{-}(g^{+}(\vec{x})) \right) \right) . \tag{10}$$

Where

$$\frac{\partial}{\partial c^{+}_{1,k,l}} \left(g^{-}(g^{+}(\vec{x})) \right) = \left(\left. \frac{\partial g^{-}_{1}}{\partial x} \right|_{x',y'}, \left. \frac{\partial g^{-}_{2}}{\partial y} \right|_{x',y'} \right) \left. \frac{\partial g^{+}_{1}}{\partial c^{+}_{1,k,l}} \right|_{x,y} . \tag{11}$$

And where

$$\vec{x} = (x, y) . \tag{12}$$

And

$$(x', y') = g^{+}(x, y) . \tag{13}$$

Again, following the definition of the transformation function we express its derivative with respect to the coefficients of the first component as

$$\frac{\partial g^{+}_{1}(x, y)}{\partial c^{+}_{1,k,l}} = \beta^{3} \left(\frac{x}{s_x} - k \right) \beta^{3} \left(\frac{y}{s_y} - l \right) . \tag{14}$$

This derivative is the same in the case of the second component.
The derivative of E^{+}_{cons} with respect to any of the deformation coefficients of the second component of the direct deformation field is calculated in an analogous way.

Let us see now the derivate of E^{+}_{cons} with respect to the coefficients of the first component of the inverse transformation:

$$\frac{\partial E^{+}_{cons}}{\partial c^{-}_{1,k,l}} = -2 \sum_{\vec{x} \in \Omega^{+}} \left(\vec{x} - g^{-}(g^{+}(\vec{x})) \right) \cdot \left(\frac{\partial}{\partial c^{-}_{1,k,l}} \left(g^{-}(g^{+}(\vec{x})) \right) \right) . \tag{15}$$

Where

$$\frac{\partial}{\partial c^{-}_{1,k,l}} \left(g^{-}(g^{+}(\vec{x})) \right) = \frac{\partial}{\partial c^{-}_{1,k,l}} \left(g^{-}(x', y') \right) = \beta^{3} \left(\frac{x'}{s_x} - k \right) \beta^{3} \left(\frac{y'}{s_y} - l \right) . \tag{16}$$

The derivative of E^{+}_{cons} with respect to any of the deformation coefficients of the second component of the inverse deformation field can be calculated in an analogous way. The derivatives of E^{-}_{cons} are easily inferred in a similar way. We refer to the original article [6] for the derivatives of E_{img}, E_{μ} and (E_{div} + E_{rot}).

2.4 Choice of w_c

All the energy terms of the functional represent different measurements over the images or the deformations, thus presenting different units. Therefore, the terms are not comparable and a weight term is needed. We determined the optimum value experimentally. While value of zero is useful to compare results with the previous algorithm, weight values around 10.0-30.0 often showed the best compromise between the final similarity and the deformation consistency for our images. Higher values make the consistency constraint too rigid and consequently decrease the images similarity. Lower values cause the lack of relevance between g^+ and g^- in the optimization process and thus do not achieve symmetric transformations. Fig. 1 shows the evolution of the similarity error with respect to w_c. The consistency error decreases with the weight but causes a significant increase in the similarity error when approaching to values close to 100.

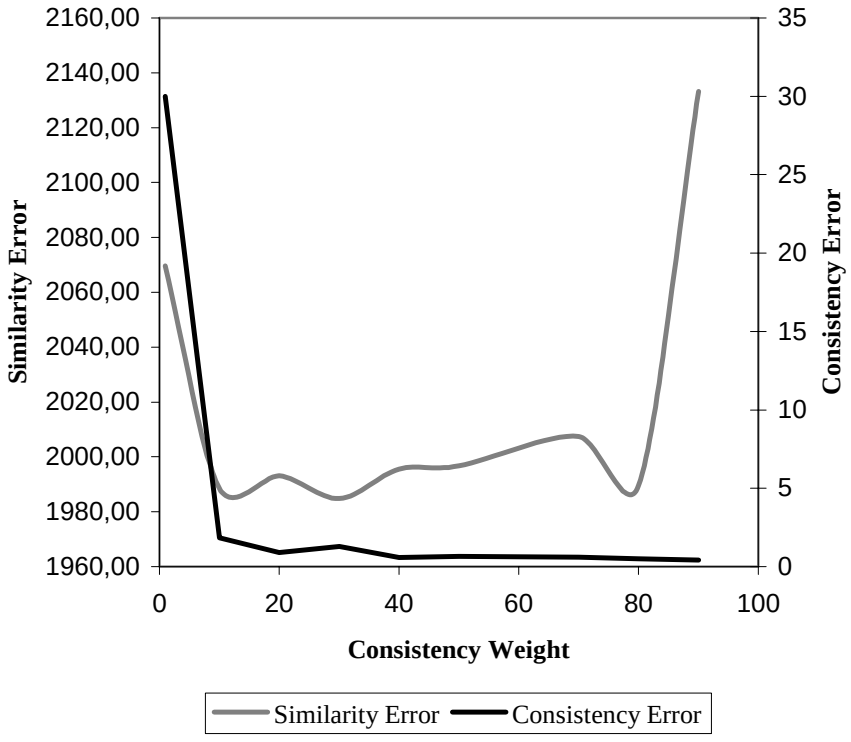

Fig. 1. Evolution of the similarity and consistency error with increasing values of the consistency weight

For the rest of weight terms we refer to [6]. From our own experience we recommend to set w_i to 1.0 and if necessary, w_μ to 1.0 and w_d and w_r to 0.1.

3 Results

To evaluate our algorithm we tested its performance using synthetic images. We applied some known deformations to the images and then checked whether our method could correct the deformation. That also allowed us to compare our algorithm with the standard one [6]. For instance, in Fig. 2 we have registered a Lena picture with a deformed version of the same image. In this case, the standard method properly registers the deformed image with the original one, but is unable to find the inverse deformation field without using soft landmarks, regularization values and a specific image mask. In the same example, our algorithm finds simultaneously both deformation fields (direct and inverse) using only the similarity term and the consistency term of the energy function.

Fig. 2. From top to down, left to right: source image, target image, registered source image (by the standard method), registered source image (by our new method), registered target image (by our new method)

Fig. 3, 4, and 5 contain a relevant example of the results obtained applying our algorithm compared to the results obtained with the original method (lacking the consistency term) using two consecutive histological sections from breast cancer tissue.

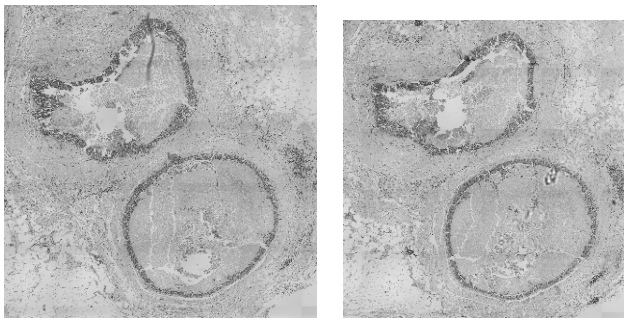

Fig. 3. Two consecutive histological sections from a human biopsy presenting two big tumors

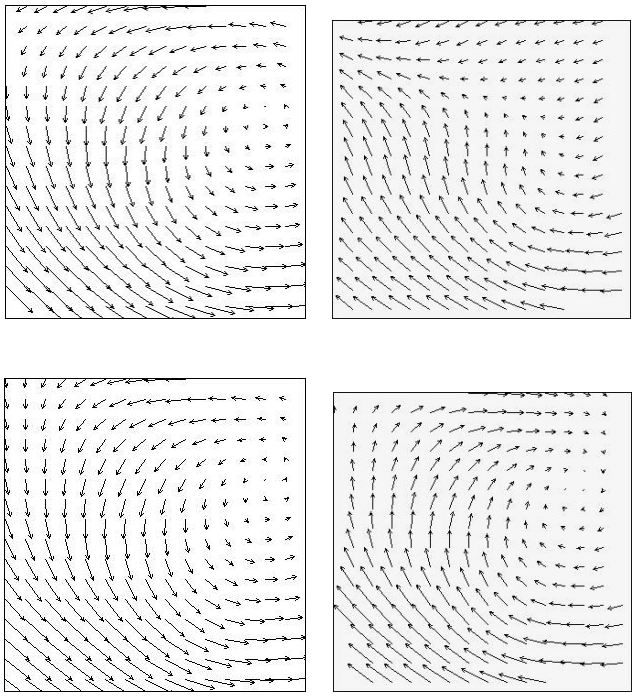

Fig. 4. Comparison of the deformation fields obtained with the original method described in [6] and our new algorithm over the images in Figure 2. The first row shows the deformation when registering image 1 to 2 (left) and image 2 to 1 (right), applying the traditional energy functional. The second row shows the same deformations when using the proposed improvement

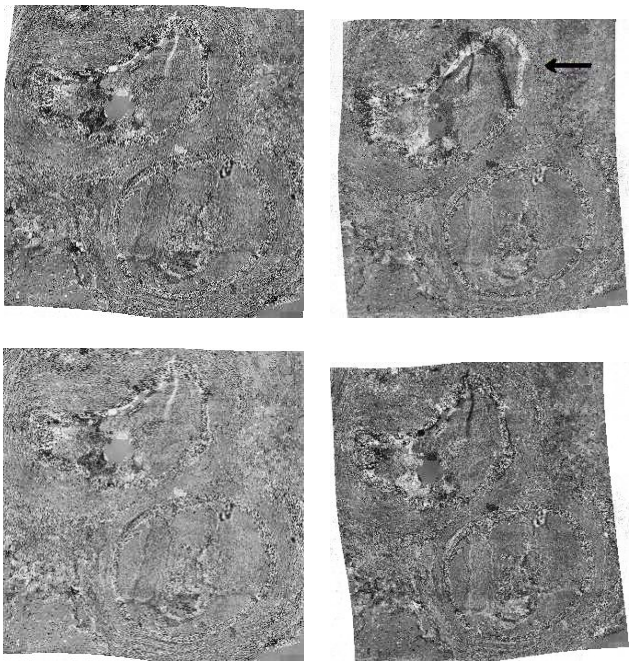

Fig. 5. The top row shows the subtractions of the deformed images and the target ones in both senses, using the traditional method. The bottom row shows the result when applying our method. The black arrow points the most relevant error committed by the standard method

Fig. 4 shows the deformation fields calculated with both methods. It is easy to see how our method guarantees the consistency between the direct and the inverse transformation while the traditional method does not.

In Fig. 5 we show the result of subtracting the deformed source and target images. We can appreciate how for the inverse transformation our method achieves a much better result than the standard method, as we expected by observing the deformation fields on Fig. 4. These results were also evaluated numerically obtaining an average of similarity error 31.63 of and 32.68 for the deformations calculated with the original method (direct-inverse and inverse-direct) and an average of 31.48 and 31.66 for the deformations of our new method. The differences between the inverse-direct averages provoke visible changes on the registration as shown in the deformation fields' representations on Fig. 4.

The grayscale sample images in Fig. 3 have respectively 325x325 pixels and 300x312 pixels and it took 18 seconds to properly register them in an Intel Pentium M, 1.60 GHz, 589 MHz, 512MB of RAM memory, under a SuSE Linux system.

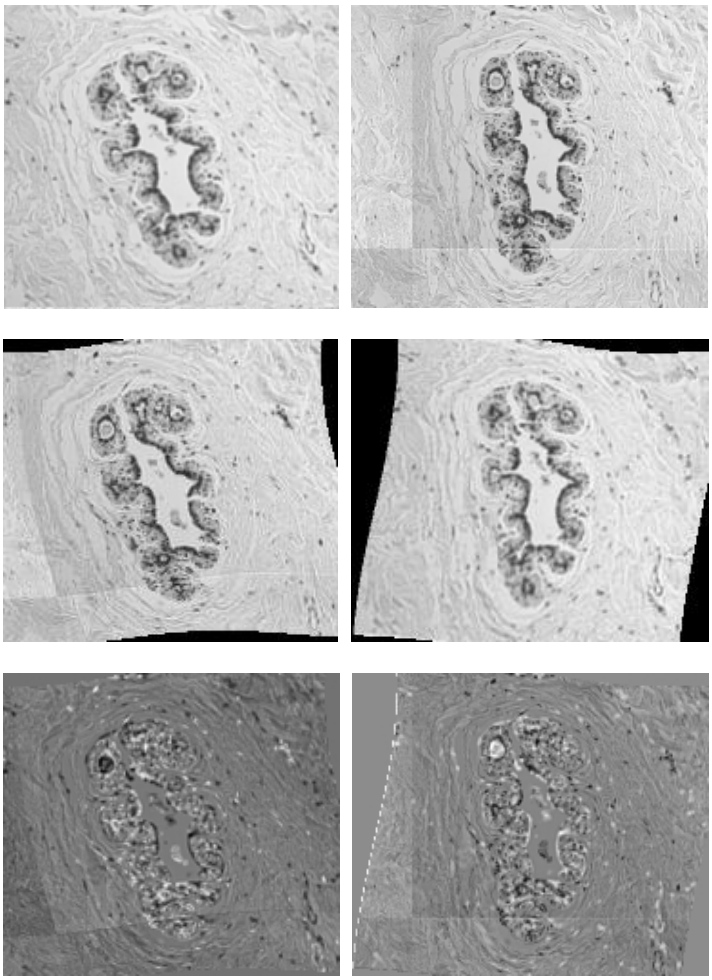

Fig. 6. Example with two transversals cuts of a mammary duct. From top to down, left to right: source image, target image, registered target image, registered source image, difference source image, difference target image

Fig. 6 is another example with breast tissue sample where the standard method is unable to approach any proper deformation between the source and target images based in the images similarity but where our new method achieves easily the right deformation thanks to the consistency term.

As inferred from the experimental results using our bidirectional method, in most cases only the similarity and the consistency term are needed to achieve a proper registration. This involves a simplification of the energy functional to be minimized and therefore, a reduction in the computational time and complexity. At the same time, forgetting about placing soft landmarks in the images allows us reducing the human interaction in the registration process, which is another advantage of our algorithm over the previous method.

4 Conclusions and Future Work

A new algorithm for consistent elastic registration has been presented. It combines the ideas of elastic image registration based on B-splines models and consistent image registration. The method improves the results obtained without the consistency factor in the energy function and accelerates the search for the optimum.

This method can be extended increasing the number of images involved in the registration to do group-wise registration. For this case, the explicit derivatives must be recalculated and a method for composing the deformation fields needs to be proposed.

5 Acknowledgments

Ignacio Arganda-Carreras is being supported by a predoctoral FPI-CAM fellowship since October 2003. Carlos Ortiz-de-Solórzano is supported by a Ramon y Cajal (Spanish Ministry of Education and Science ryc-2004-002353) and a Marie Curie International Reintegration Grant (FP6-518688). Jan Kybic was sponsored by the Czech Ministery of Education under project number MSM210000012. Partial support is acknowledged to Comunidad de Madrid through grant GR/SAL/0234, to Instituto de Salud Carlos III-Fondo de Investigaciones Sanitarias (FIS) through the IM3 Network and grant 040683 and to the Plan Nacional de Investigación Científica, Desarrollo e Innovación Tecnológica (I+D+I).

References

1. Fernandez-Gonzalez, R., Jones, A., Garcia-Rodriguez, E., Chen, P.Y., Idica, A., Barcellos-Hoff, M.H. and Ortiz-de-Solorzano, C.: A System for Combined Three-Dimensional Morphological and Molecular Analysis of Thick Tissue Specimens, Microscope Research and Technique 59(6): 522-530, 2002.
2. Fernandez-Gonzalez, R., Deschamps, T., Idica, A., Malladi, R. and Ortiz-de-Solorzano, C.: Automatic segmentation of histological structures in mammary gland tissue sections, Journal of Biomedical Optics, vol. 9, pp. 444-453, 2004.
3. Hajnal, J. V., Hill, D. L. G., and Hawkes, D. J.: Eds., Medical image registration, CRC Press, 2001.
4. Maintz, J. B. A. and Viergever, M. A.: A survey of medical image registration, Medical Image Analysis, vol. 2, no. 1, pp. 1–36, 1998.
5. Arganda-Carreras, I., Fernandez-Gonzalez, R. and Ortiz-de-Solorzano, C.: Automatic Registration Of Serial Mammary Gland Sections, The 26th International Conference of the IEEE Engineering in Medicine and Biology Society (EMBS), 1-5th September, 2004, San Francisco, California.

6. Sorzano, C.O.S., Thevenaz, P. and Unser, M.: Elastic Registration of Biological Images Using Vector-Spline Regularization. IEEE Transactions on Biomedical Engineering, vol. 52, no. 4, pp. 652-663, April 2005.
7. Christensen, G.E. and He, J.: Consistent nonlinear elastic image registration, Mathematical Methods in Biomedical Image Analysis, MMBIA 2001, IEEE.